Micro-Roughness Effects in (Elasto)Hydrodynamic Lubrication Including a Mass-Flow Preserving Cavitation Model

Guy Bayada

INSA de Lyon / LAMCOS CNRS-UMR 5514 / ICJ CNRS-UMR 5208
Bât. Léonard de Vinci, 21 av. Jean Capelle
69621 Villeurbanne cedex, France

Sébastien Martin

INSA de Lyon / ICJ CNRS-UMR 5208
Bât. Léonard de Vinci, 21 av. Jean Capelle
69621 Villeurbanne cedex, France

Carlos Vázquez

Universidade da Coruña
Facultade de Informática / Dept. de Matemáticas
Campus Elviña, 15071-A Coruña, España

Abstract

An average Reynolds equation is proposed for predicting the effects of deterministic periodic roughness, taking JFO mass flow preserving cavitation model and elasto-hydrodynamic effects into account. For this, the asymptotic model is based upon a double scale analysis approach. The average Reynolds equation can be used both for the description of cavitation on a macroscopic scale in widening gap regions as well as for cavitation on the microscopic interasperity scale. Results of numerical simulations based on the model are presented for the case of a hydrodynamically lubricated journal bearings and an elasto-hydrodynamically lubricated point contact.

Key words: Elastohydrodynamic; Lubrication; Roughness.

Email addresses: guy.bayada@insa-lyon.fr (Guy Bayada), sebastien.martin@insa-lyon.fr (Sébastien Martin), carlosv@udc.es (Carlos Vázquez).

Preprint *20 February 2007*

NOMENCLATURE

h_r	=	rigid gap
$h_{[p]}$	=	effective gap (including deformation)
h_0	=	minimum thickness of the rigid gap
R	=	sphere or cylinder section radius
k	=	Hertz kernel
p	=	pressure
p_0, $p_1 \ldots$	=	approximations of the pressure
θ	=	saturation
θ_0	=	microscopic average saturation
Θ_i, Θ	=	macro-average saturations
$x = (x_1, x_2)$	=	space variables
$y = (y_1, y_2)$	=	microscale variables
$Y =]0,1[\times]0,1[$	=	rescaled microcell
$(A^\star_{[p]})_{ij}$, $B^{(i,\star)}_{[p]}$	=	average coefficients
$w^{(i)}_{[p_0]}$, $\chi^{(i,0)}_{[p_0]}$	=	auxiliary functions defined on Y
α	=	piezoviscosity coefficient
$\partial/\partial n$	=	normal derivative
ε	=	roughness spacing
$\overline{\cdot}^Y$	=	average operator with respect to y
L	=	length of the journal bearing
R_b, R_j, R_m	=	bearing radius, journal radius, mean radius
Γ_a, Γ_0, $\Gamma_\sharp$, $\Gamma_\star$	=	boundaries of the device
c, ρ	=	clearance, eccentricity of the bearing
p_a	=	supply pressure
μ	=	viscosity
v_0	=	velocity of the bearing
a_r	=	amplitude of the roughness
W	=	load
θ_{in}	=	supply flow

1 Introduction

In this paper, it is explained how the double scale procedure, already used to obtain average equations with periodic roughness in the case of rigid bearings [1–3], can be extended to EHD problems including cavitation and starvation. The JFO mass flow preserving model is used, including pressure and saturation as unknown functions. This model takes into account both microcavitation (due to the microroughness) and macrocavitation (due to the diverging part of the gap). The average equation can be easily solved for some specific roughness patterns (transverse, longitudinal) exactly in the same way as the initial EHD problem with cavitation. Numerical results are given for both purely hydrodynamic and EHD point-contact problems, for a two dimensional device.

2 Basic equations

Our studied cavitation model, like the Elrod algorithm and its variants [4,5], views the film as a mixture. It does not, however, make the assumption of liquid compressibility in the full film area as in [6] and some other papers [7]. In this general framework, the effective gap between the two close surfaces, denoted $h_{[p]}$, contains a given rigid contribution h_r and an elastic one, which strongly depends on the main unknown p (lubricant pressure) in the following nonlocal form:

$$h_{[p]}(x) = h_r(x) + \int_\Omega k(x,z)p(z)\,dz,$$

the kernel k depending on the kind of contact. The classical approximation of the rigid gap [8] is given by the expression

$$h_r(x) = \begin{cases} h_0 + \dfrac{x_1^2 + x_2^2}{2R}, & \text{for point contacts,} \\ h_0 + \dfrac{x_1^2}{R}, & \text{for line contacts,} \end{cases} \tag{1}$$

that represents a parabolic approximation for a given sphere-plane (point contact) or cylinder-plane (line contact) gap, R being the sphere or cylinder section radius. In the point contact case, the positive constant h_0 corresponds to the gap at the point nearest to contact while, in the line contact case, it includes a constant related to the logarithmic kernel (see [9] for instance). Now,

let us introduce the general property of the kernel k:

$$k(x,z) = \begin{cases} c_0 \ \log\left|\dfrac{c_1 - z_1}{x_1 - z_1}\right|, & \text{for line contacts,} \\ \dfrac{c_0}{\sqrt{(x_1 - z_1)^2 + (x_2 - z_2)^2}}, & \text{for point contacts,} \end{cases} \tag{2}$$

where $c_0 > 0$ and $c_1 \geq \max\{\left|x_1\right|,\ x \in \overline{\Omega}\}$. The flow obeys the following "universal" Reynolds equation (here written in a dimensionless form):

$$\sum_{i=1}^{2} \frac{\partial}{\partial x_i}\left(h_{[p]}^3\ e^{-\alpha p}\ \frac{\partial p}{\partial x_i}\right) = \frac{\partial\ \theta h_{[p]}}{\partial x_1}, \tag{3}$$

$$p \geq 0, \quad 0 \leq \theta \leq 1, \quad p\,(1-\theta) = 0, \tag{4}$$

p is the pressure (assumed to be a positive function), θ is the relative mixture density, $h_{[p]}$ the real film thickness, x_1 is the direction of the effective relative shear velocity of the device, while x_2 is the transverse direction. Here, the pressure cavitation is assumed to be zero. Moreover, the lubricant is piezoviscous so that the viscosity obeys the Barus law (notice that other laws may be taken into account), α being the piezoviscosity parameter.

3 Asymptotic expansion

3.1 General case in the elastohydrodynamic configuration

Let us suppose that the roughness is periodically reproduced in the two x_1 and x_2 directions from an elementary cell Y (or "miniature bearing" in Tonder's terminology). Relatively to this elementary cell Y, we define the microscopic

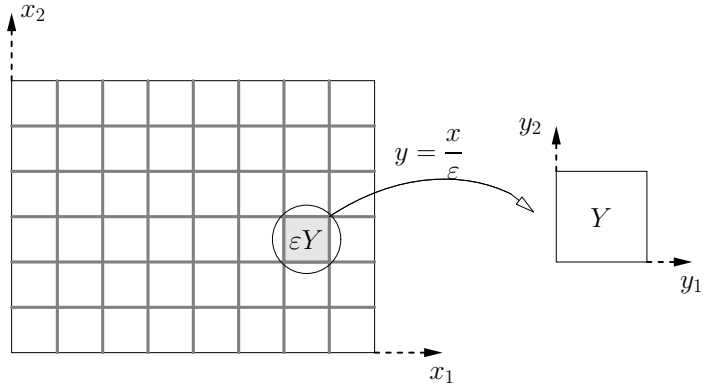

Fig. 1. Macroscopic domain and elementary cells

variables $y = (y_1, y_2)$ such that $Y = \{0 < y_1 < 1,\ 0 < y_2 < y_2\}$ which is used to describe the oscillatory effects (see FIG. 1).

Let us now consider gaps that can be written as $h_r(x, y)$. In this section, we use the two-scale analysis which has been widely developped for the hydrodynamic case in [3]. The equations should be read as

$$\sum_{j=1}^{2} \frac{\partial}{\partial x_j} \left\{ \left(h_{[p]}(x, y) \right)^3 e^{-\alpha p(x)} \frac{\partial p}{\partial x_j}(x) \right\} = \frac{\partial}{\partial x_1} \left\{ \theta(x)\, h_{[p]}(x, y) \right\},$$
$$p(x) \geq 0, \quad 0 \leq \theta(x) \leq 1, \quad p(x)\,(1 - \theta(x)) = 0,$$

with the additional notation:

$$h_{[p]}(x, y) = h_r(x, y) + \int_{\Omega} k(x, z)\ p(z)\ dz.$$

Let us introduce the parameter ε which denotes the period of the roughness patterns: the fast variables (y_1, y_2) describe oscillatory effects induced by the roughness patterns, namely

$$(y_1, y_2) := \left(\frac{x_1}{\varepsilon}, \frac{x_2}{\varepsilon} \right)$$

Thus, similarly to the hydrodynamic case (studied in [3]), we shall look for an asymptotic expansion of the solutions:

$$p(x) = p_0(x) + \varepsilon p_1(x, y) + \varepsilon^2 p_2(x, y) + ..., \tag{5}$$
$$\theta(x) = \theta_0(x, y), \tag{6}$$

p_0 being a positive function, and each unknown p_i $(i \geq 1)$ and θ_0 being function of (x, y). The problem of the boundary conditions to be satisfied by the p_i is somewhat difficult but may be summarized so:

(i) The natural boundary conditions on (p, θ) are assigned to p_0 and an equivalent saturation linked to θ_0.
(ii) The functions p_i, $i \geq 1$, are Y periodic, i.e. periodic in the two variables y_1, y_2, for each value of (x_1, x_2).

To be noticed that, unlike of p, we do not introduce an asymptotic expansion for θ. This can be explained by observing the evolution of p and θ as ε tends to 0. Clearly, the oscillations of the pressure are decreasing and p tends to a smooth function (namely p_0 which, actually, does not depend on the fast variable). This is not the case for θ and an asymptotic smooth limit cannot be

considered. Moreover, from the initial properties of the pressure-saturation, the following ones hold:

$$p_0(x) \geq 0, \quad 0 \leq \theta_0(x,y) \leq 1, \quad p_0(x,y)\,(1-\theta_0(x,y)) = 0. \tag{7}$$

Using the two-scale analysis [1,3], we obtain the micro-macroscopic link between the unknowns p_0, p_1 and θ_0:

$$p_1(x,y) = e^{\alpha p_0(x)}\,\chi^{(1,0)}_{[p_0]}(x,y) - \sum_{i=1}^{2} \frac{\partial p_0}{\partial x_i}(x)\; w^{(i)}_{[p_0]}(x,y), \tag{8}$$

in which $w^{(i)}_{[p_0]}$, $\chi^{(i),0}_{[p_0]}$ (and, additionally, $\chi^{(i,\star)}_{[p_0]}$) $(i = 1,2)$ are the Y periodic solutions (up to an additive constant) of the following local problems (see [3] for the rigorous introduction of these local problems):

$$\sum_{j=1}^{2} \frac{\partial}{\partial y_j}\left(h^3_{[p_0]}\; e^{-\alpha p_0}\; \frac{\partial w^{(i)}_{[p_0]}}{\partial y_j} \right) = \frac{\partial h^3_{[p_0]}}{\partial y_i}, \tag{9}$$

$$\sum_{j=1}^{2} \frac{\partial}{\partial y_j}\left(h^3_{[p_0]}\; e^{-\alpha p_0}\; \frac{\partial \chi^{(i,0)}_{[p_0]}}{\partial y_j} \right) = \frac{\partial \theta_0 h_{[p_0]}}{\partial y_i}, \tag{10}$$

$$\sum_{j=1}^{2} \frac{\partial}{\partial y_j}\left(h^3_{[p_0]}\; e^{-\alpha p_0}\; \frac{\partial \chi^{(i,\star)}_{[p_0]}}{\partial y_j} \right) = \frac{\partial h_{[p_0]}}{\partial y_i}. \tag{11}$$

Notice that, contrary to the local problems in the purely hydrodynamic case which have been studied in [3], the local problems in the EHL problem highly depend on the macroscopic pressure p_0, which is due to the piezoviscosity and elastic deformation. These local problems describe the link between the unknowns at the microscopic scale, the macroscopic one playing the role of a parameter. To complete the results, we obtain the following average Reynolds equation, taking into account the roughness effects. There are now three leading unknowns $(p_0, \Theta_1, \Theta_2)$ satisfying the following equations:

$$\sum_{i,j=1}^{2} \frac{\partial}{\partial x_i}\left\{ \left(A^{\star}_{[p_0]}\right)_{ij} e^{-\alpha p_0} \frac{\partial p_0}{\partial x_j} \right\} = \sum_{i=1}^{2} \frac{\partial}{\partial x_i}\left\{ \Theta_i B^{(i,\star)}_{[p_0]} \right\}, \tag{12}$$

$$p_0 \geq 0, \quad p_0(1-\Theta_i) = 0, \quad (i = 1,2), \tag{13}$$

where the average coefficients are given by:

$$\left(A^{\star}_{[p_0]}\right)_{ij} = \overline{h^3_{[p_0]}\,\delta_{ij} - h^3_{[p_0]}\frac{\partial w^{(i)}_{[p_0]}}{\partial y_j}}^{Y},$$
$$B^{(i,\star)}_{[p_0]} = \overline{h_{[p_0]}\,\delta_{1i} - h^3_{[p_0]}\frac{\partial \chi^{(1,\star)}_{[p_0]}}{\partial y_i}}^{Y},$$

δ_{ij} denoting the Kronecker symbol (δ_{ij} has value 1 for $i = j$, 0 for $i \neq j$). Equations (12) and (13) deal with any periodic roughness pattern. To be noticed is the fact that the differential operator is no more of the Reynolds type since extra terms $\partial^2 p_0/\partial x_i \partial x_j$ appear. The right-hand side also contains an additive term in the x_2 direction. Moreover, it is possible to prove in a rigorous way [10] that there exists a solution with an isotropic saturation $\Theta = \Theta_1 = \Theta_2$ and $0 \leq \Theta \leq 1$. Under some additional assumptions (see [3]), we can even prove some complementary results, which are presented in the next subsections.

3.2 Particular cases in the elastohydrodynamic configuration

When dealing with transverse roughness and longitudinal roughness, the average coefficients can be easily simplified and given in an explicit form. In both cases, the asymptotic system has the same structure than the initial (smooth) one, i.e.

$$\sum_{i=1}^{2}\frac{\partial}{\partial x_i}\left\{A^{(i,\star)}_{[p_0]}\; e^{-\alpha p_0}\frac{\partial p_0}{\partial x_i}\right\} = \frac{\partial \Theta B^{(1,\star)}_{[p_0]}}{\partial x_1}, \tag{14}$$
$$p_0 \geq 0, \quad 0 \leq \Theta \leq 1, \quad p_0\,(1-\Theta) = 0. \tag{15}$$

▷ *Transverse roughness*: the average coefficients are

$$A^{(1,\star)}_{[p_0]} = \frac{1}{\overline{h^{-3}_{[p_0]}}^{Y}}, \quad A^{(2,\star)}_{[p_0]} = \overline{h^3_{[p_0]}}^{Y}, \quad B^{(1,\star)}_{[p_0]} = \frac{\overline{h^{-2}_{[p_0]}}^{Y}}{\overline{h^{-3}_{[p_0]}}^{Y}},$$

the link between the macroscopic saturation Θ and the microscopic one θ_0 being given by:

$$\Theta = \frac{1}{\overline{h^{-2}_{[p_0]}}^{Y}}\;\overline{\left(\frac{\theta_0}{h^2_{[p_0]}}\right)}^{Y}.$$

▷ *Longitudinal roughness*: the average coefficients are

$$A_{[p_0]}^{(1,\star)} = \overline{h_{[p_0]}^3}^Y, \quad A_{[p_0]}^{(2,\star)} = \frac{1}{\overline{h_{[p_0]}^{-3}}^Y}, \quad B_{[p_0]}^{(1,\star)} = \overline{h_{[p_0]}}^Y,$$

the link between the macroscopic saturation Θ and the microscopic one θ_0 being given by:

$$\Theta = \frac{\overline{\theta_0 h_{[p_0]}}^Y}{\overline{h_{[p_0]}}^Y}.$$

All the earlier results are valid for both elastohydrodynamic and hydrodynamic cases and, thus, generalize the ones that have been stated in [3]. As an important feature, Θ is not the average of the microscopic saturation θ_0 but contains some anisotropic effects due to the roughness direction.

3.3 Particular cases in the hydrodynamic configuration

In the purely hydrodynamic case, one can prove some additional results, corresponding to a wide class of two dimensional roughness patterns. Indeed, suppose that h_r can be written under the form

$$h_r(x,y) = h_1(x,y_1)\, h_2(x,y_2),$$

then we get the following (hydrodynamic) average equation

$$\sum_{i=1}^{2} \frac{\partial}{\partial x_i}\left\{ A_{ii}^{(\star)} \frac{\partial p_0}{\partial x_i} \right\} = \frac{\partial}{\partial x_1}\left\{ \Theta B^{(1,\star)} \right\},$$
$$p_0 \geq 0, \quad 0 \leq \Theta \leq 1, \quad p_0(1-\Theta) = 0,$$

with

$$A_{ii}^{(\star)} = \frac{\overline{h_j^3}^Y}{\overline{h_i^{-3}}^Y}, \quad \text{for } i,j = 1,2 \text{ and } i \neq j, \qquad B^{(1,\star)} = \frac{\overline{h_1^{-2}}^Y}{\overline{h_1^{-3}}^Y}\, \overline{h_2}^Y,$$

the link between the micro-macroscopic saturations being given by

$$\Theta = \frac{1}{\overline{h_2}^Y\, \overline{h_1^{-2}}^Y} \overline{\left(\frac{\theta_0 h_2}{h_1^2} \right)}^Y.$$

4 Numerical results

In this section, the numerical simulation of a micro(elasto)hydrodynamic contact is performed to illustrate the theoretical results of convergence stated in the previous sections. For the numerical solution of the ε-dependent problems and their corresponding average one, the algorithm is based on the Bermudez-Moreno method : a characteristics method coupled to a duality method, adapted to steady state problems dealing with a finite element spatial discretization, is used in order to treat the nonlinearity related to cavitation phenomena. Piezoviscous effects and elastic deformation of the surfaces are taken into account by a standard fixed-point method. These numerical techniques have been already successfully used in previous papers dealing with hydrodynamic aspects (see [11,12]), and elastohydrodynamic aspects (see, for instance, [13,14]). It has been proved that, for small loads, it is a rigorous method whose numerical solution converges to the continuous one, as the mesh size tends to 0. In TABLE 1, we present the functional coefficients

$$A^{(1,\star)}_{[p_0]}, \quad A^{(2,\star)}_{[p_0]}, \quad B^{(1,\star)}_{[p_0]}$$

that appear in the average problem for purely transverse and purely longitudinal roughness cases which have been partially computed with MAPLE. Suppose that the domain to be considered is a rectangular one $(a,b)\times(c,d)$, and that the rough (elasto)hydrodynamic gap can be written under the form

$$h_{[p]}\left(x,\frac{x}{\varepsilon}\right) = h_r(x)+h_d[p](x)+\begin{cases} \alpha_1 \sin\left(\dfrac{2\pi}{\varepsilon}\dfrac{x_1-a}{b-a}\right), & \text{(transverse roughness)} \\ \alpha_2 \sin\left(\dfrac{2\pi}{\varepsilon}\dfrac{x_2-c}{d-c}\right), & \text{(longitudinal roughness)} \end{cases}$$

where h_r (resp. $h_d[p]$) denotes the smooth rigid (resp. elastic) contribution to the gap and the remaining term describes the roughness patterns in the purely transverse or longitudinal case.

	Transverse roughness	Longitudinal roughness
$h_{[p]}(x,y)$	$h_r(x)+h_d[p](x)+\alpha_1\sin(2\pi y_1)$	$h_r(x)+h_d[p](x)+\alpha_2\sin(2\pi y_2)$
$A^{(1,\star)}_{[p_0]}$	$2\dfrac{\left((h_r+h_d[p])^2-\alpha_1^2\right)^{5/2}}{2(h_r+h_d[p])^2+h_r^2}$	$(h_r+h_d[p])^3+\dfrac{3}{2}\,(h_r+h_d[p])\,\alpha_2^2$
$A^{(2,\star)}_{[p_0]}$	$(h_r+h_d[p])^3+\dfrac{3}{2}\,(h_r+h_d[p])\,\alpha_1^2$	$2\,\dfrac{\left((h_r+h_d[p])^2-\alpha_2^2\right)^{5/2}}{2(h_r+h_d[p])^2+\alpha_2^2}$
$B^{(1,\star)}_{[p_0]}$	$2(h_r+h_d[p])\,\dfrac{(h_r+h_d[p])^2-\alpha_1^2}{2(h_r+h_d[p])^2+\alpha_1^2}$	$h_r+h_d[p]$

Table 1
Elastohydrodynamic average coefficients

4.1 Hydrodynamic case

We adress the numerical simulation of journal bearing devices with circumferential supply of lubricant. The mechanical characteristics of the device are given by:

- length: $L = 0.019\ m$,
- bearing radius: $R_b = 0.0164975\ m$,
- journal radius: $R_j = 0.01647\ m$,
- mean radius: $R_m = 0.5\ (R_b + R_j)$,
- clearance : $c = R_b - R_j$,
- eccentricity: $\rho = 0.2$.

The physical characteristics of the regime are the following ones:

- supply pressure: $p_a = 283000\ Pa$,
- lubricant viscosity: $\mu = 0.02\ Pa.s$,
- shear velocity: $v_0 = 17.247\ m/s$.

The earlier problem leads to the following set of equations

$$\sum_{i=1}^{2} \frac{\partial}{\partial x_i}\left(h^3\ \frac{\partial p}{\partial x_i}\right) = \Lambda \frac{\partial\ \theta h}{\partial x_1},$$
$$p \geq 0, \quad 0 \leq \theta \leq 1, \quad p\ (1-\theta) = 0,$$

with $\Lambda = 6\mu v_0$, and the real smooth gap shoud be read as

$$h(x) = c\,(1 + \rho\ \cos\left(x_1/R_m\right)).$$

The equations have to be solved on the domain $(0, 2\pi R_m) \times (0, L/2)$ (see the developped configuration on FIG.2) with the following boundary conditions:

- $p = p_a$ on Γ_a, $p = 0$ on Γ_0,
- conditions on $\Gamma_\sharp$: p and $\Lambda\,\theta h - h^3 \dfrac{\partial p}{\partial x_1}$ are $2\pi R_m x_1$ periodic.

To be noticed is the fact that the corresponding average boundary conditions can be written as follows (using the terminology of TABLE 1):

- $p_0 = p_a$ on Γ_a, $p_0 = 0$ on Γ_0,
- conditions on $\Gamma_\sharp$: p_0 and $\Lambda\,\Theta B^{(1,\star)} - A^{(1,\star)} \dfrac{\partial p_0}{\partial x_1}$ are $2\pi R_m x_1$ periodic.

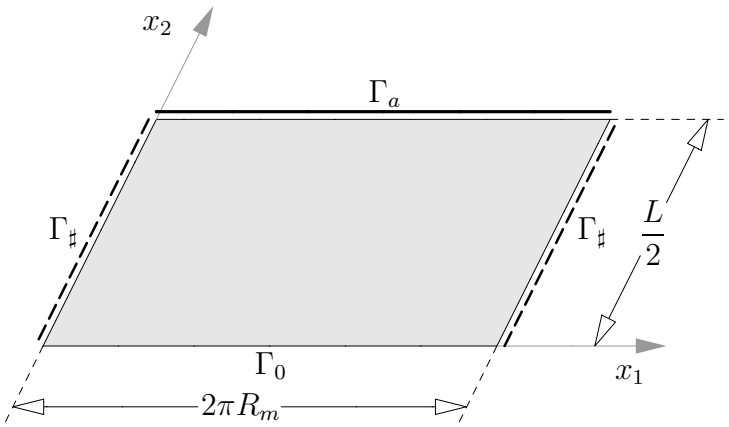

Fig. 2. Journal bearing domain

Actually, we consider transverse roughness patterns and the gap should be read as:

$$h\left(x, \frac{x}{\varepsilon}\right) = c\left(1 + \rho\ \cos\left(x_1/R_m\right) + a_r\ \sin\left(\frac{2\pi}{\varepsilon}\frac{x_1}{R_m}\right)\right)$$

with $a_r/\rho = 0.2$, a_r denoting the amplitude parameter of the roughness. Numerical tests have been made with a mesh grid containing 201*51 elements, which is proved to be sufficient in terms of numerical convergence. As there is at most 30 roughness patterns in the x_1 direction, this has lead to a mesh discretization of 7 points at least for each roughness pattern. Moreover, numerical results remain the same when using meshes with size 401*51 or 201*101.

Fig.3 and 4 (resp. 5 and 6) show the pressure and saturation profiles for $\varepsilon = 1/15$ (resp. $\varepsilon = 1/30$) compared to the average solution, at a fixed $x_2^0 = L/4$. Thus, it allows to observe the roughness effects in the x_1 direction. The amplitude of the pressure oscillations tend to be damped, although the amplitude of the saturation oscillations stay the same in cavitated areas. As it was noticed in [3], it points out the fact that when the number of roughness patterns increases, the pressure behaves as a smooth function, namely $p_0(x)$, while the saturation behaves as a highly oscillating function, namely $\theta_0(x, x/\varepsilon)$. Thus, the pressure tends to a smooth one as ε tends to 0, while the saturation is always oscillating. To be noticed on Fig.4 and 6 is the fact that the cavitation area is made of two macrocavitation zones (for $\varepsilon = 1/15$, $x_1 > 0.06$ and $x_1 < 0.01$) and a lot of microcavitation zones. Fig.7 and 8 represent the average pressure and saturation in the real domain.

Let us notice that the average process, that we have presented here, only allows a macroscopic description of the microscopic roughness effects as the number of patterns is large: in particular, interasperity cavitation cannot be predicted in the average model, which only describes the (macro-) cavitation regions for

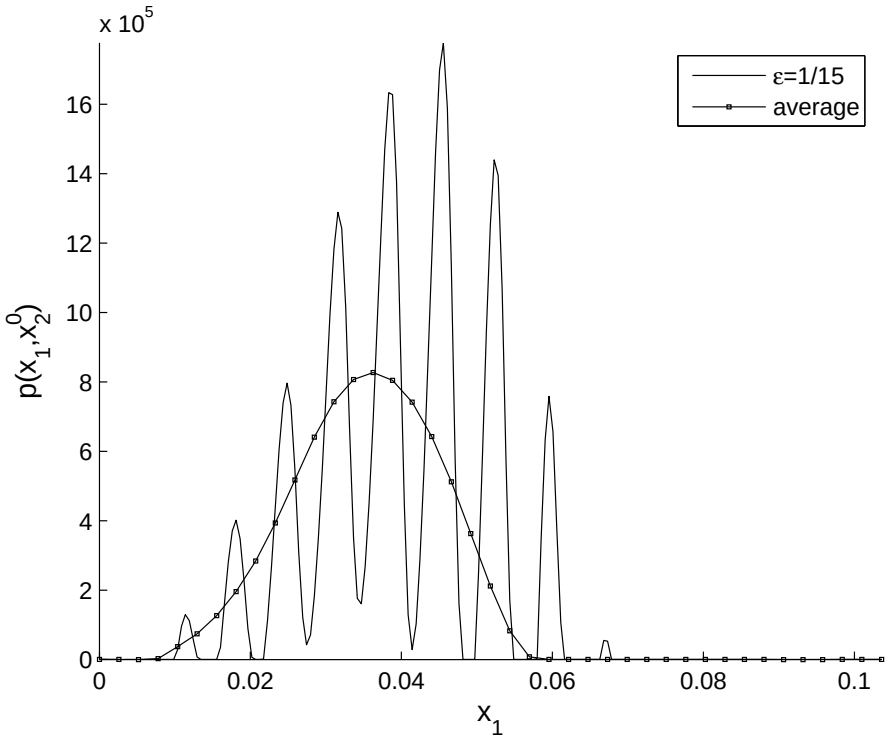

Fig. 3. Hydrodynamic pressure for $\varepsilon = 1/15$ at $x_2^0 = L/4$

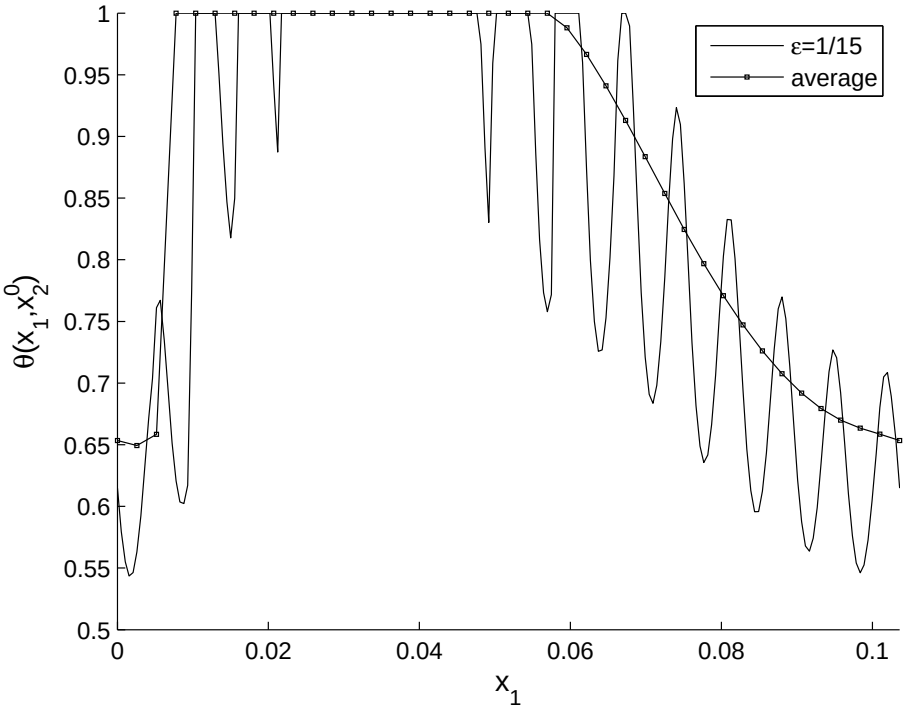

Fig. 4. Hydrodynamic saturation for $\varepsilon = 1/15$ at $x_2^0 = L/4$

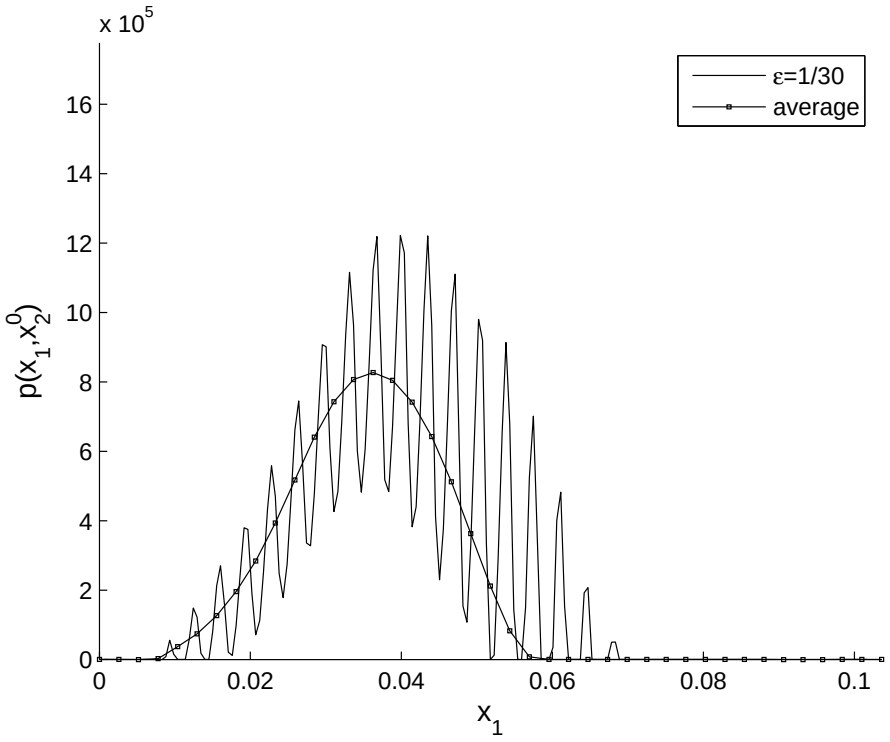

Fig. 5. Hydrodynamic pressure for $\varepsilon = 1/30$ at $x_2^0 = L/4$

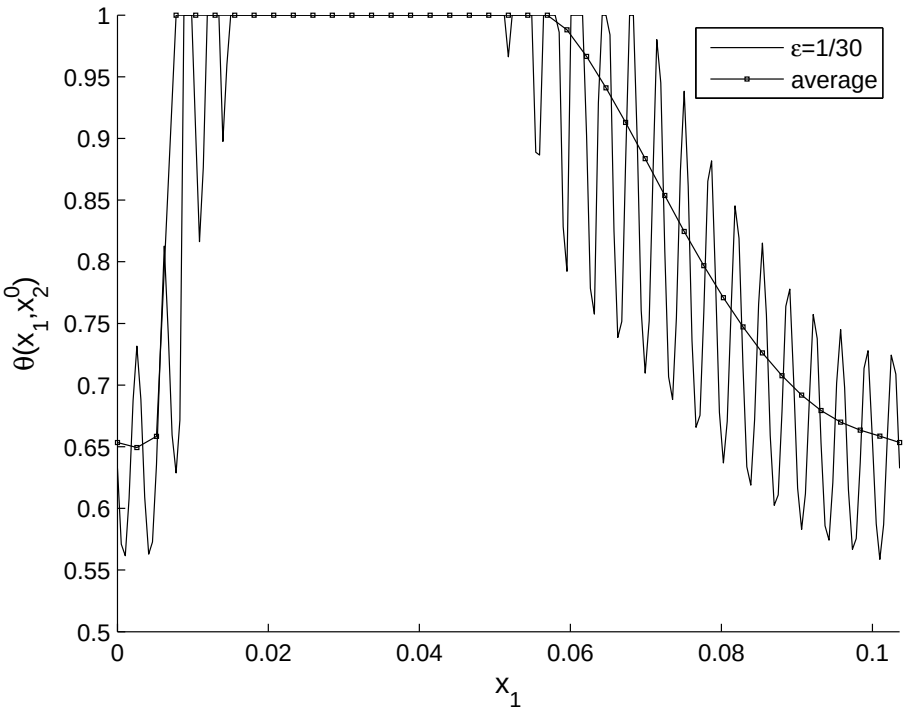

Fig. 6. Hydrodynamic saturation for $\varepsilon = 1/30$ at $x_2^0 = L/4$

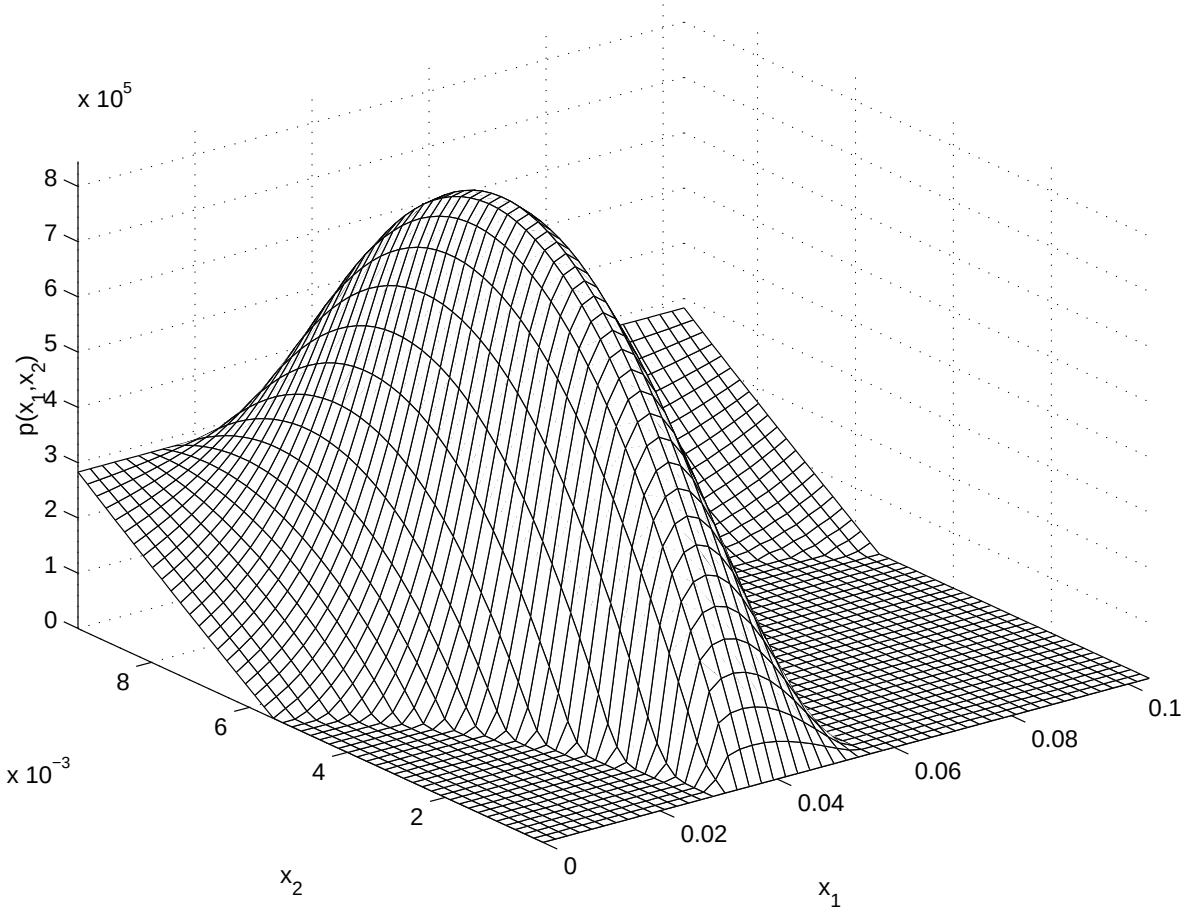

Fig. 7. Average hydrodynamic pressure in the whole device

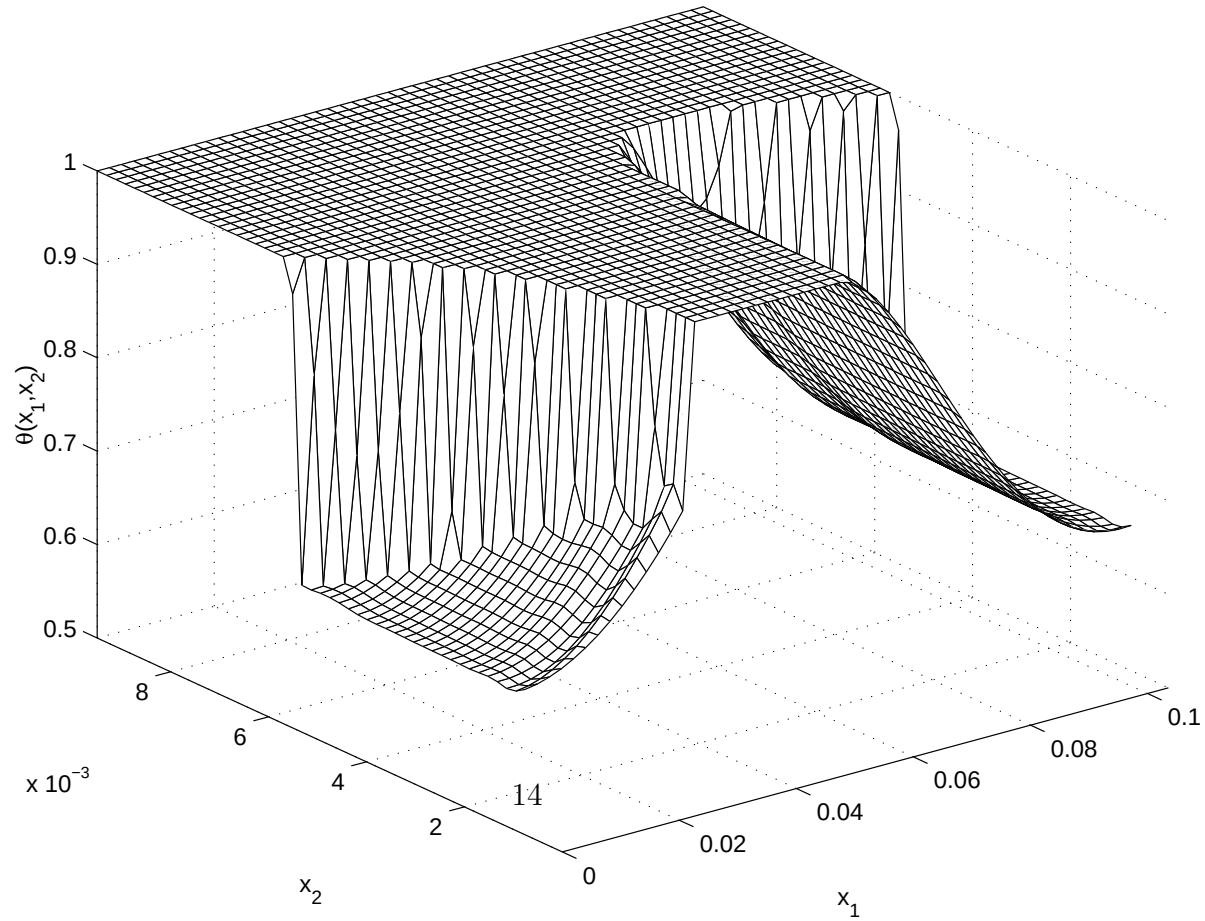

Fig. 8. Average hydrodynamic saturation in the whole device

a large number of roughnesses. Additional information on interasperity cavitation is contained in the supplementary terms of the asymptotic expansion of the pressure, namely $p_1(x, y)$, for which little information is known.

4.2 Elastohydrodyamic case

The numerical tests deal with a dimensionless problem, as described in Section 2: the domain is $(-4, 2) \times (2, 2)$. The considered rigid contribution to the gap is a normalized one:

$$h_0 + \frac{x_1^2 + x_2^2}{2}$$

where h_0 denotes the minimum thickness. Since a point contact has been considered, we choose the following Hertz model:

$$k(x, z) = \frac{2}{\pi^2} \frac{1}{\sqrt{(x_1 - z_1)^2 + (x_2 - z_2)^2}}$$

The equations are:

$$\sum_{i=1}^{2} \frac{\partial}{\partial x_i} \left(h[p]^3 \; e^{-\alpha p} \; \frac{\partial p}{\partial x_i} \right) = \frac{\partial \; \theta h[p]}{\partial x_1},$$
$$p \geq 0, \quad p \; (1 - \theta) = 0 \quad 0 \leq \theta \leq 1,$$

The boundary conditions are the following ones:

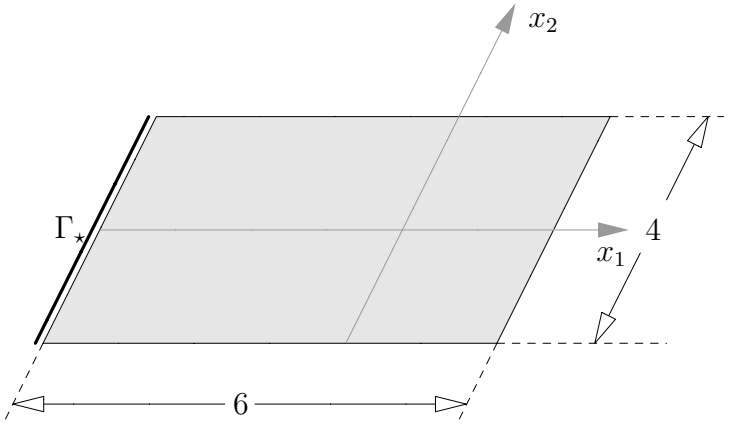

Fig. 9. Normalized EHL domain

- flow condition on $\Gamma_\star$: $\theta h[p] - h[p]^3 \dfrac{\partial p}{\partial x_1} = \theta_{in} h[p]$, with $\theta_{in} = 0.3$,
- $p = 0$ elsewhere.

The corresponding average boundary conditions can be written as:

- flow condition on $\Gamma_\star$: $\Theta B^{(1,\star)}_{[p_0]} - A^{(1,\star)}_{[p_0]} \dfrac{\partial p_0}{\partial x_1} = \theta_{in} C^{(\star)}_{[p_0]}$, with $C^{(\star)}_{[p_0]} = (h_r + h_d[p])_{|\Gamma_\star}$.
- $p_0 = 0$ elsewhere.

The chosen values of h_0 and α will be discussed further.

4.2.1 Transverse roughness

Numerical tests deal with the following rigid contribution to the gap:

$$h_0 + \frac{x_1^2 + x_2^2}{2} + h_0 \ \sin\left(2\pi \frac{x_1 + 4}{6\ \varepsilon}\right)$$

with $h_0 = 0.5$ and different values of ε. Moreover, the piezoviscosity has been taken to $\alpha = 1$. This numerical configuration corresponds to a very small load contact. Computations have been made for different values of ε (with at most $1/\varepsilon = 30$ roughness patterns), and the mesh grid which has been used contains 201*51 elements, as in the hydrodynamic case. The average coefficients in the transverse roughness cases are deduced from TABLE 1 (see page 9).

FIG.10–11 (resp. 12–13) provide the pressure-saturation profiles at $x_2^0 = 0$ with $\varepsilon = 1/20$ (resp. $\varepsilon = 1/30$) compared to the average solution. To be observed is the fact that the average profiles give a satisfying approach of the roughness effects ($\varepsilon = 1/30$): indeed, the pressure profiles given in FIG.10 and 12 evidence the fact that the average pressure is a smooth version of the rough pressure. Similarly, by FIG.11 and 13, the average saturation can be seen as an average version of the rough saturation, up to anisotropic effects. On FIG.16, we observe that the deformation corresponding to $\varepsilon = 1/30$ nearly coincides with the average one: this is due to the regularizing effects of the Hertz kernel. In fact, the deformation profile has a rate of convergence which is much greater than the pressure profile. FIG.14, 15 and 17 represent the average pressure, saturation and deformation in the domain.

Again, similarly to the hydrodynamic computations, the average model does not provide any information of cavitation occurring at the microscopic level: it only means that the effective pressure is closer and closer to the average (smooth) pressure as the number of roughness patterns increases (i.e. ε tends to 0) but it does not provide information of micro-cavitation for a given value of ε.

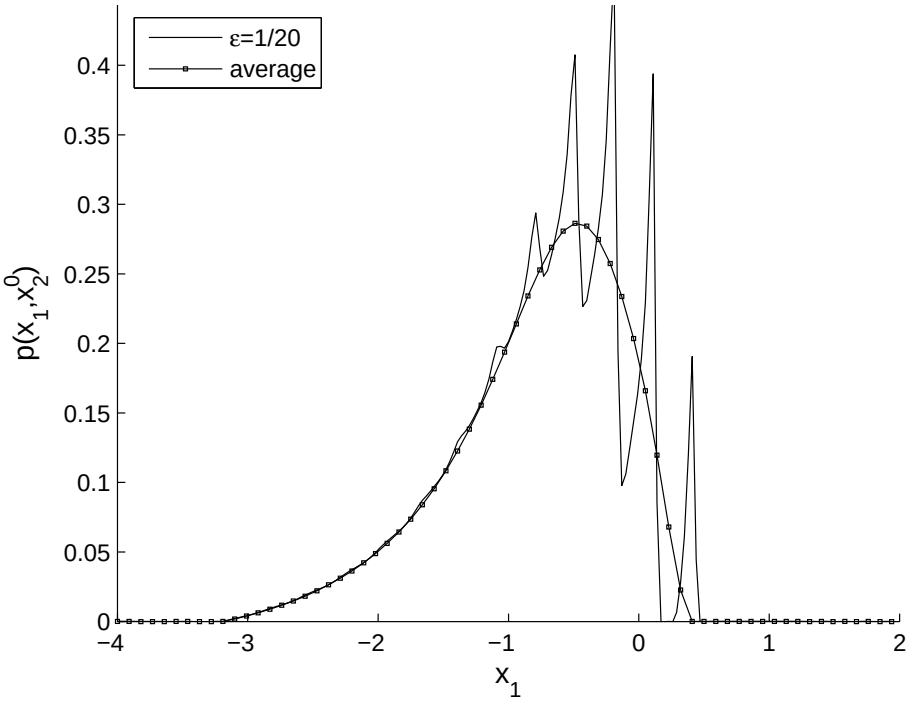

Fig. 10. EHL pressure with transverse patterns at $x_2^0 = 0$, $\varepsilon = 1/20$

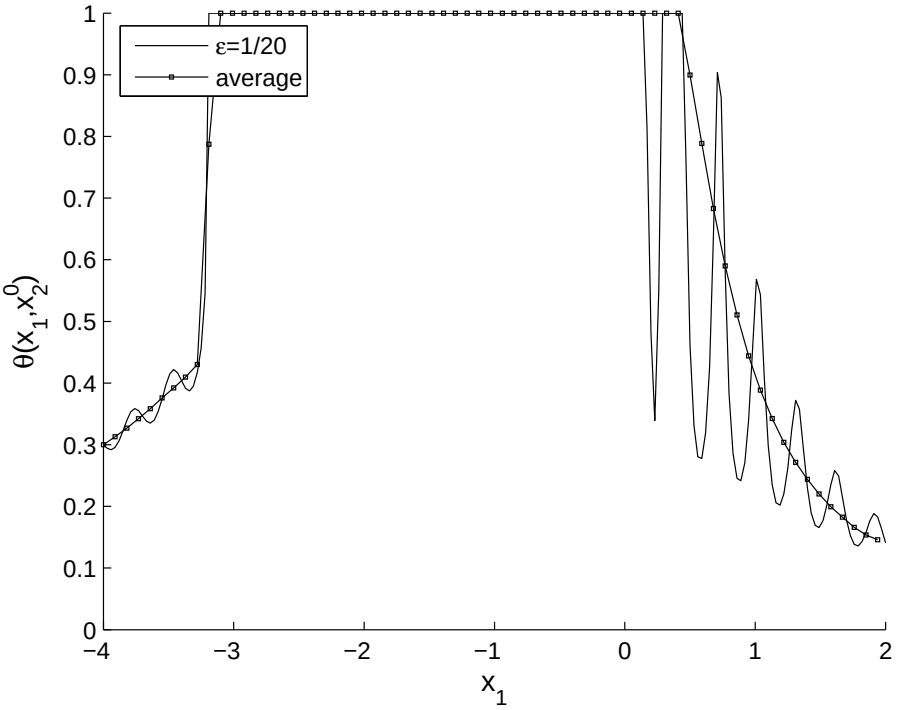

Fig. 11. EHL saturation with transverse patterns at $x_2^0 = 0$, $\varepsilon = 1/20$

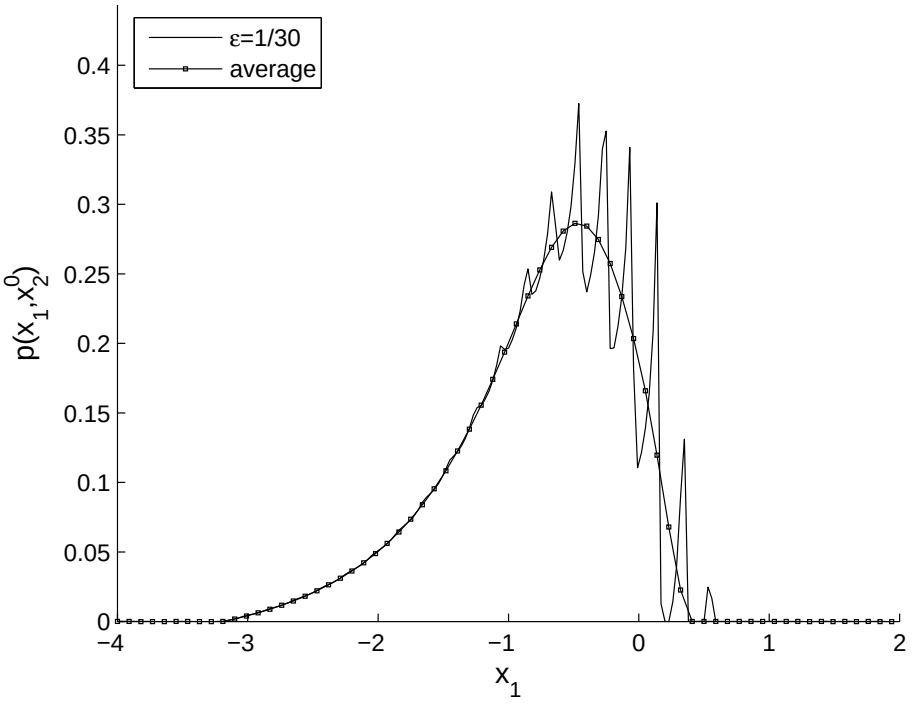

Fig. 12. EHL pressure with transverse patterns at $x_2^0 = 0$, $\varepsilon = 1/30$

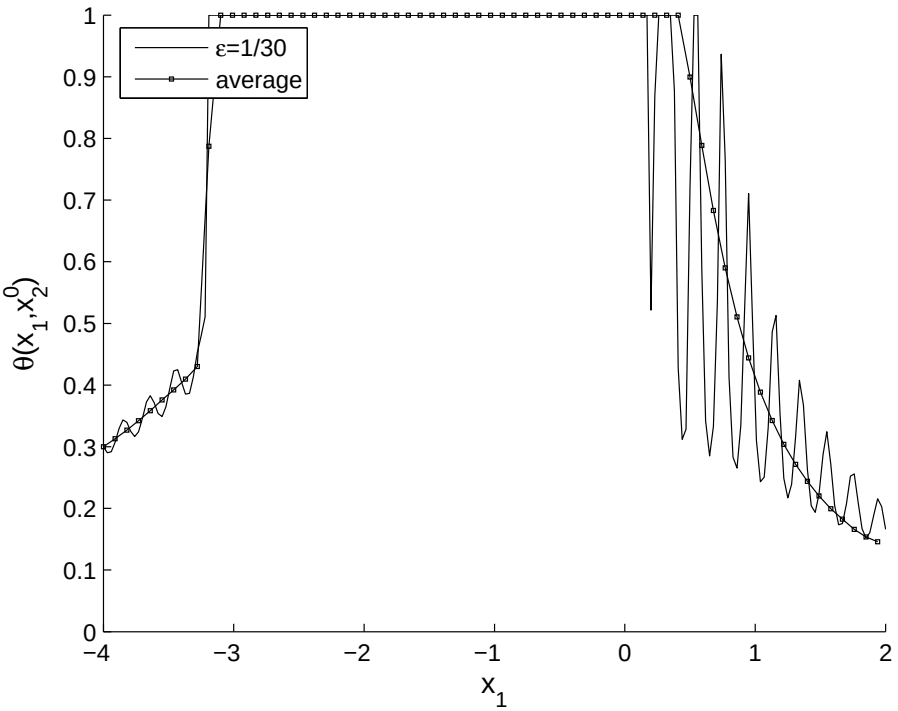

Fig. 13. EHL saturation with transverse patterns at $x_2^0 = 0$, $\varepsilon = 1/30$

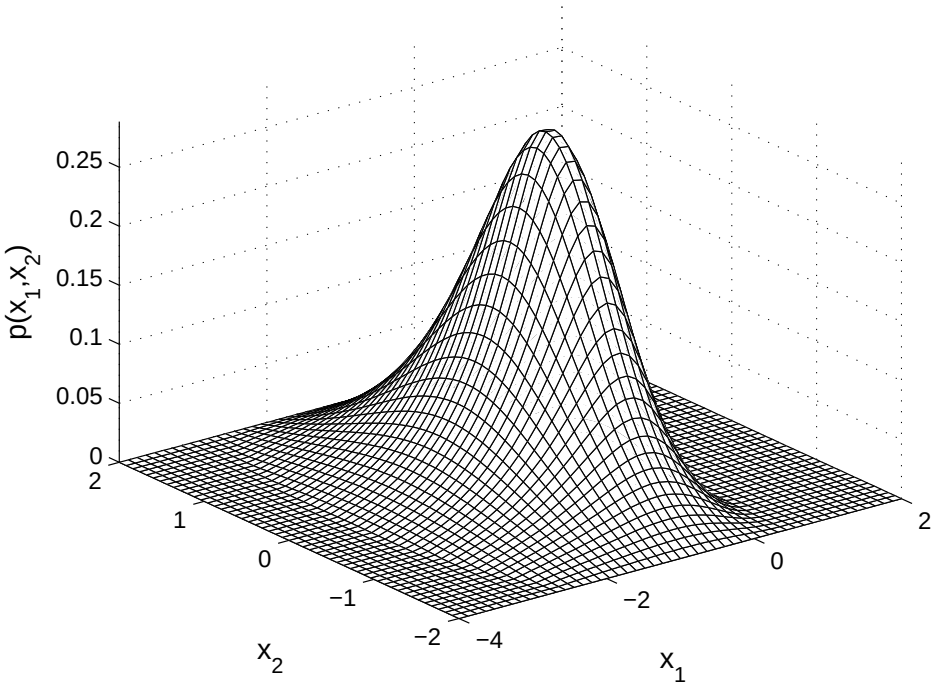

Fig. 14. EHL average pressure with transverse patterns in the whole domain

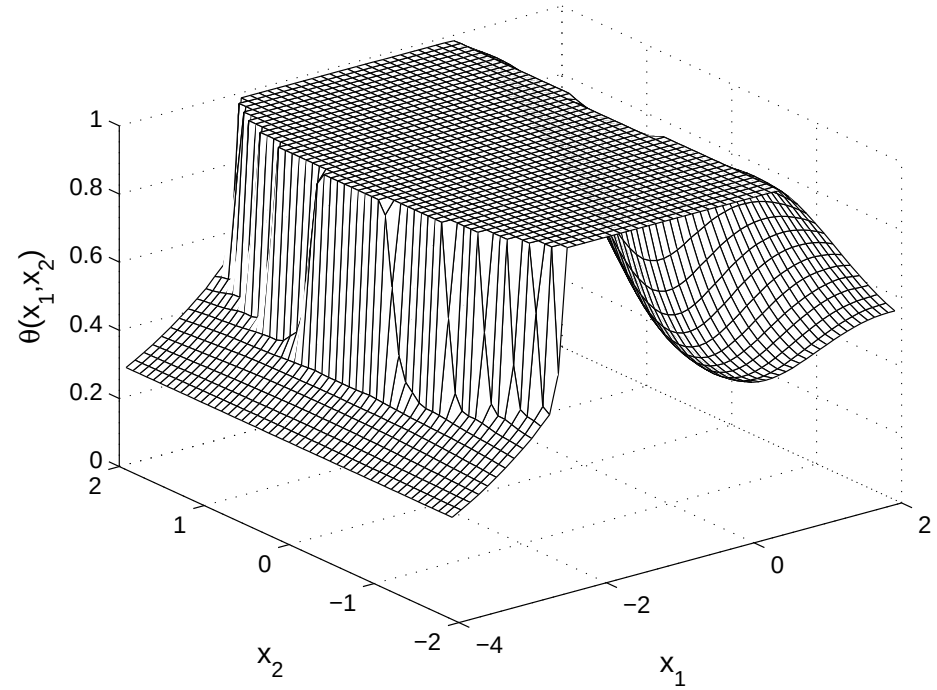

Fig. 15. EHL average saturation with transverse patterns in the whole domain

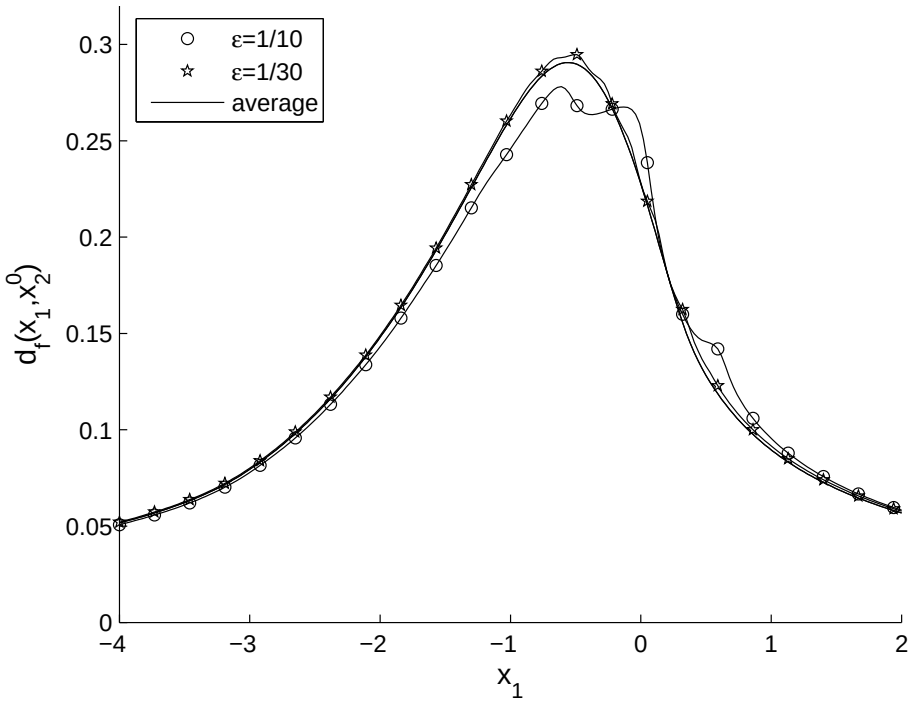

Fig. 16. EHL deformation with transverse roughness patterns at $x_2^0 = 0$

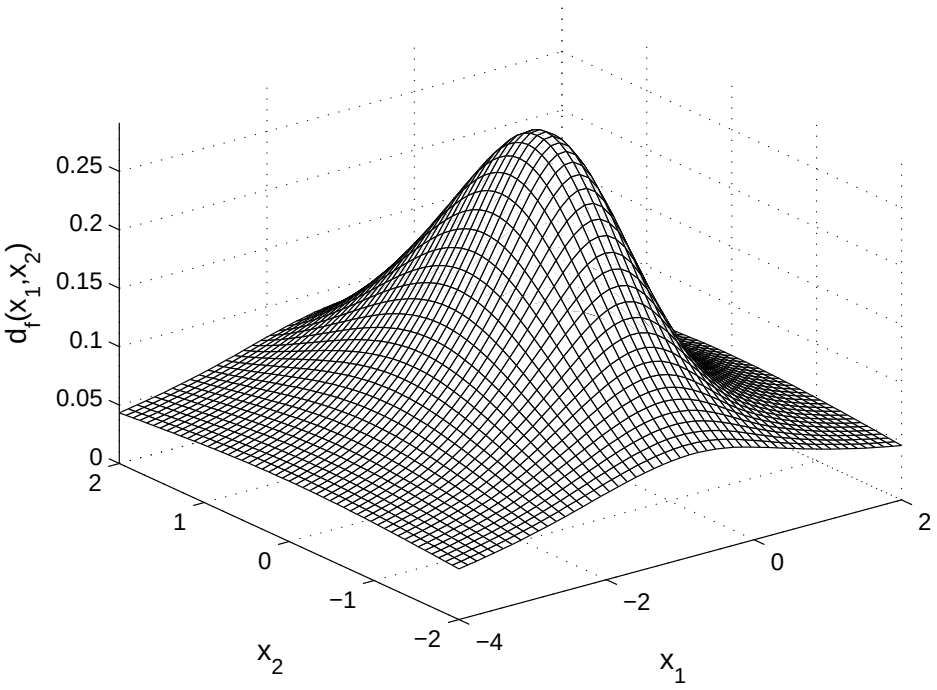

Fig. 17. Average EHL deformation in the whole domain

4.2.2 Longitudinal roughness

Numerical tests have been made for the following rigid contribution to the gap:

$$h_0 + \frac{x_1^2 + x_2^2}{2} + h_0 \ \sin\left(2\pi \frac{x_2 + 2}{4\ \varepsilon}\right)$$

with $h_0 = 0.5$ and different values of ε. Moreover, the piezoviscosity has been taken to $\alpha = 1$. Let us notice that, again, average coefficients in the transverse roughness cases are deduced from TABLE 1 (see page 9).

Computations have been made for different values of ε (with at most $1/\varepsilon = 30$ roughness patterns), with a mesh grid which containing 51*201 elements: the discretization has been refined in the x_2 direction in order to take into account the roughness effects in this direction.

FIG.18 and 19 represent the pressure and deformation profiles at $x_1^0 = -0.4$, in the x_2 direction (in order to observe the roughness effects). This choice corresponds to the maximum pressure in the average case, which is attained at $(x_1^0, x_2^0) = (-0.4, 0)$. Of course, the saturation profile is omitted, for all corresponding saturation functions would be identically equal to 1 (no cavitation in this part of the domain). Significantly, the size of the oscillations for the pressure are damped easily, and convergence of the rough solution to the average one is illustrated on both figures. Similarly, pressure / saturation / deformation curves are omitted, for they are similar to the ones observed in the transverse roughness case.

4.2.3 Influence of the roughness effects in EHL and hydrodynamic cases

FIG.20 and 21 show the difference of roughness effects between a purely hydrodynamic (isoviscous) configuration and an elastohydrodynamic (piezoviscous) configuration. The numerical and physical data are the same as in the transverse roughness case (see Subsection 4.2.1), except for the rough gap whose amplitude of roughness patterns is modified in order to prevent contact between the surfaces in the hydrodynamic case: thus, the gap is

$$h_0 + \frac{x_1^2 + x_2^2}{2} + 0.7\ h_0 \ \sin\left(2\pi \frac{x_1 + 4}{6\ \varepsilon}\right),$$

all other numerical data being the same as before (in particular for the value of h_0 and the piezoviscosity parameter α). It can be noticed that the elevation of the pressure due to the roughness patterns is less important in the EHL case than in the purely hydrodynamic case. This is due to the fact that the elastic deformation tends to damp the additional load corresponding to the

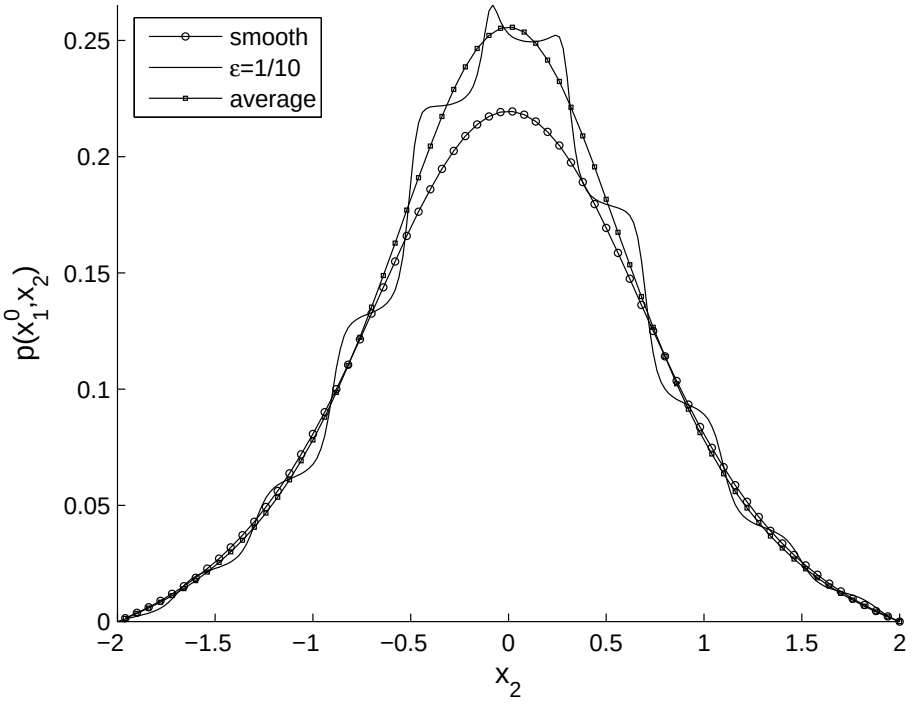

Fig. 18. EHL pressure with longitudinal patterns at $x_1^0 = -0.4$

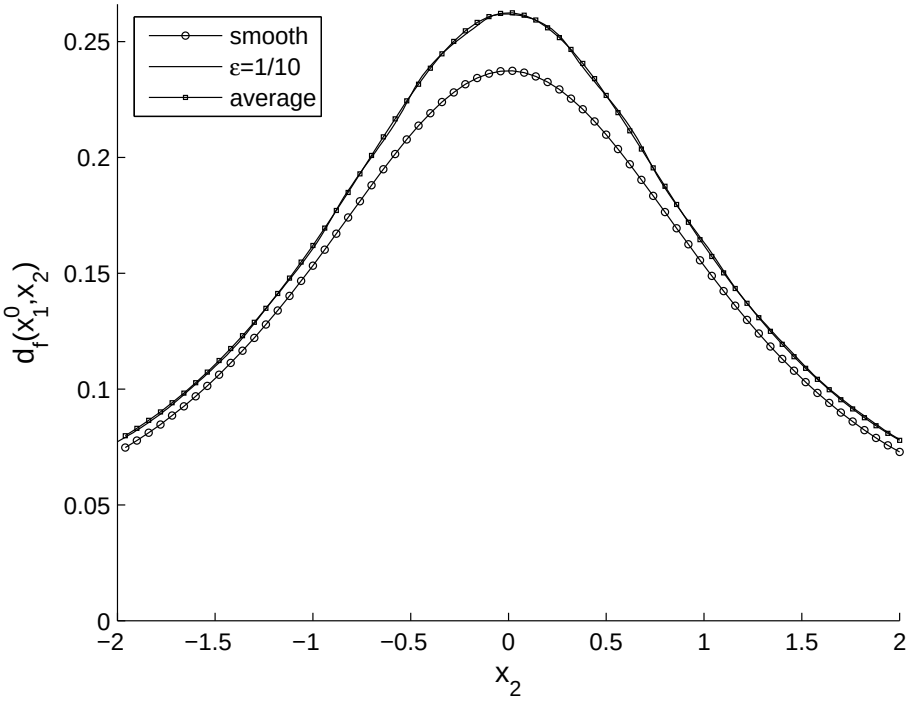

Fig. 19. EHL deformation with longitudinal patterns at $x_1^0 = -0.4$

roughness. It has little influence over the saturation distribution, although the homogenization process does not allow to get microcavitation effects which do exist when a deterministic rough pattern is considered. Though, this analysis also states that microcavitation effects tend to vanish as ε tends to 0.

4.2.4 Influence of the roughness over the load

Numerical tests have been made for the following rigid contribution to the gap:

$$h_0 + \frac{x_1^2 + x_2^2}{2} + a_r \ \sin\left(2\pi \frac{x_1 + 4}{6\ \varepsilon}\right)$$

with $h_0 \in \{0.5, 1, 1.5, 2\}$ and $a_r/h_0 \in \{0.2, 0.4, 0.6, 0.8, 1\}$. Moreover, the elastic contribution to the gap is the one given at the beginning of Subsection 4.2, and piezoviscosity has been taken to $\alpha = 0$ (isoviscous case). Results have been obtained with a mesh grid 101*101. They are given on FIG.22, showing the influence of the minimum thickness $h_r - a_r$ over the load W for different values of h_0. Results are taken from the analysis of the corresponding average solution.

4.2.5 Influence of the piezoviscosity

We focus on the behaviour of the solution with respect to the piezoviscosity parameter α. Numerical and physical data are the same than in the elastohydrodynamic case with transverse roughness (Subsection 4.2.1), except that we take into account piezoviscous properties of the lubricant: $\alpha = 0$, 1, 2 or 3.

FIG.23 and 24 represent the pressure and deformation profiles at $x_2^0 = 0$ in the average case. They illustrate the trend induced by the piezoviscosity parameter: the peak pressure and the peak deformation increase with α. Only a few variations affect the saturation distribution (for this reason, the corresponding curves are omitted).

TABLE 2 (resp. TABLE 3) gives the variation of the peak pressure (resp. deformation) with respect to the isoviscous case ($\alpha = 0$) in different rough cases (including smooth and average ones).
The relative variation of the peak pressure is denoted

$$\Delta p/p = \frac{\max(p^\alpha) - \max(p^0)}{\max(p^0)}$$

where p^α (resp. p^0) denotes the pressure distribution corresponding to the piezoviscous regime $\alpha \neq 0$ (resp. isoviscous regime $\alpha = 0$). Similarly, the

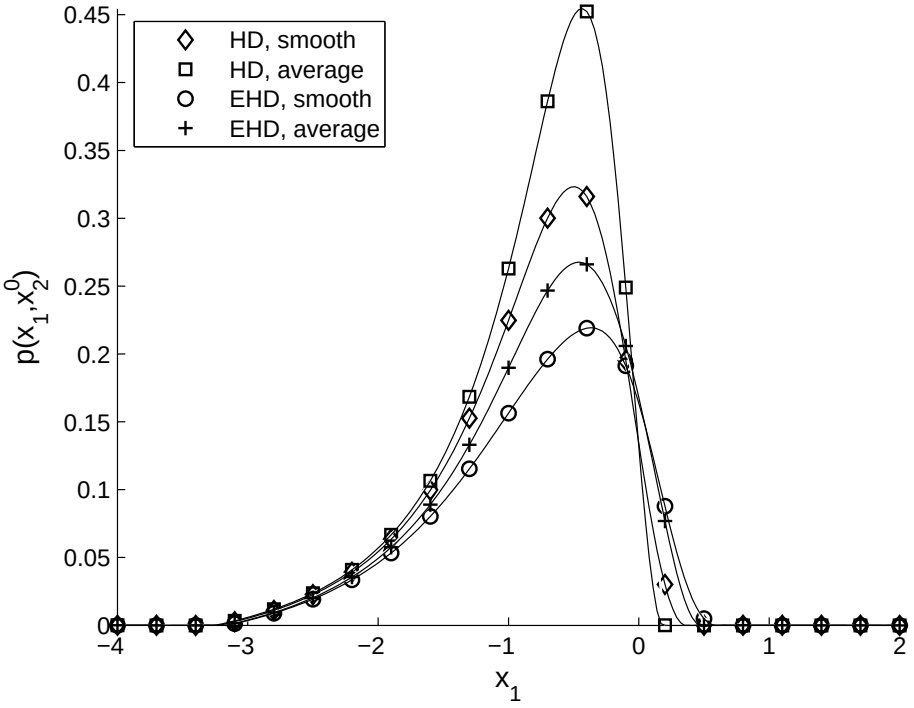

Fig. 20. Transverse roughness effects over the pressure in purely hydrodynamic and elastohydrodynamic cases at $x_2^0 = 0$

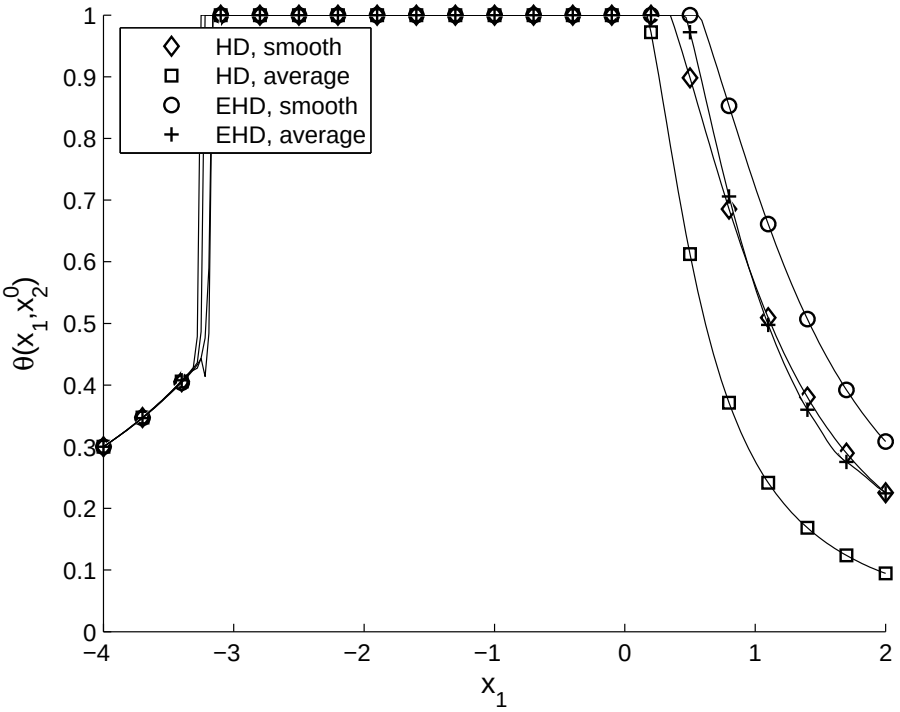

Fig. 21. Transverse roughness effects over the saturation in purely hydrodynamic and elastohydrodynamic cases at $x_2^0 = 0$

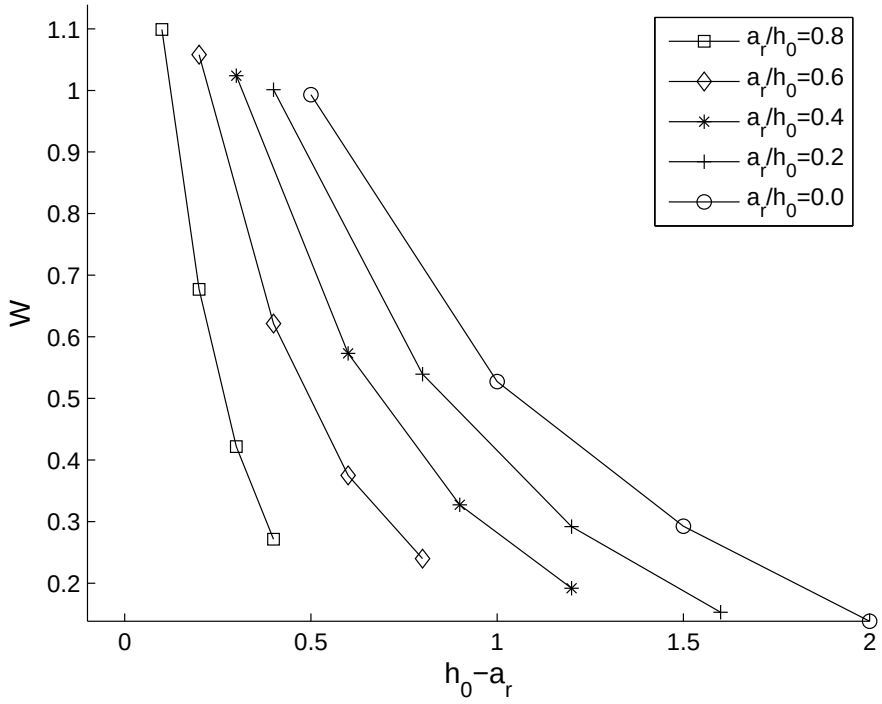

Fig. 22. Influence of the roughness over the load

relative variation of the peak deformation is denoted

$$\Delta d/d = \frac{\max(d_f^\alpha) - \max(d_f^0)}{\max(d_f^0)}$$

where d_f^α (resp. d_f^0) denotes the deformation distribution corresponding to the piezoviscous regime $\alpha \neq 0$ (resp. isoviscous regime $\alpha = 0$).

$\Delta p/p$	$\alpha = 1$	$\alpha = 2$	$\alpha = 3$
smooth	0.0817	0.2633	0.4449
$\varepsilon = 1/10$	0.1035	1.8646	2.8203
$\varepsilon = 1/20$	0.2447	0.6551	1.0192
$\varepsilon = 1/30$	0.1855	0.5161	1.3783
average	0.1041	0.3030	0.5543

Table 2
Maximum pressure elevation due to piezoviscosity

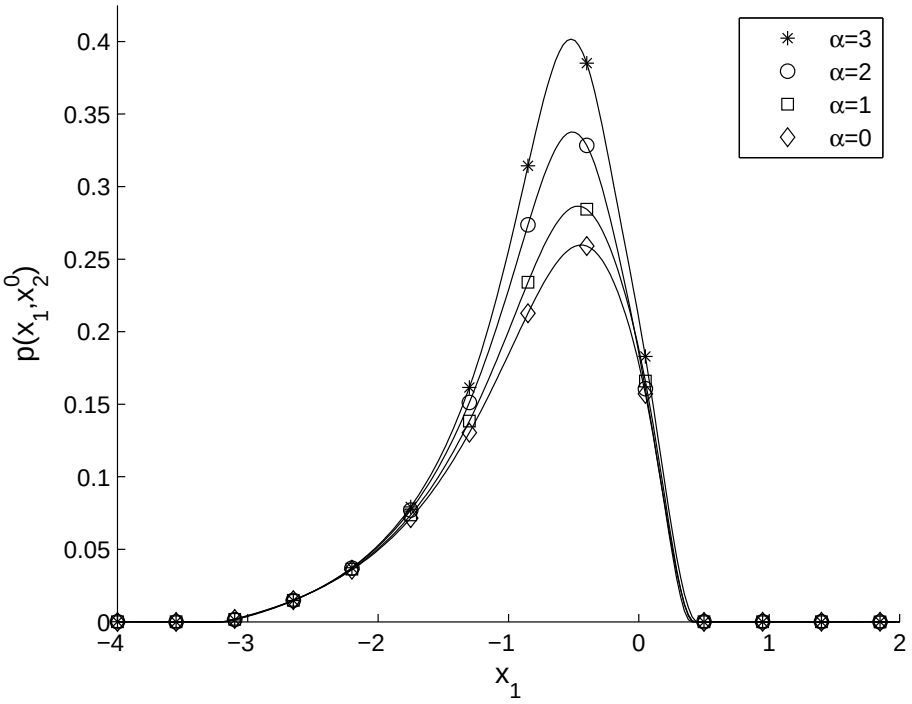

Fig. 23. Influence of the piezoviscosity over the (average) pressure

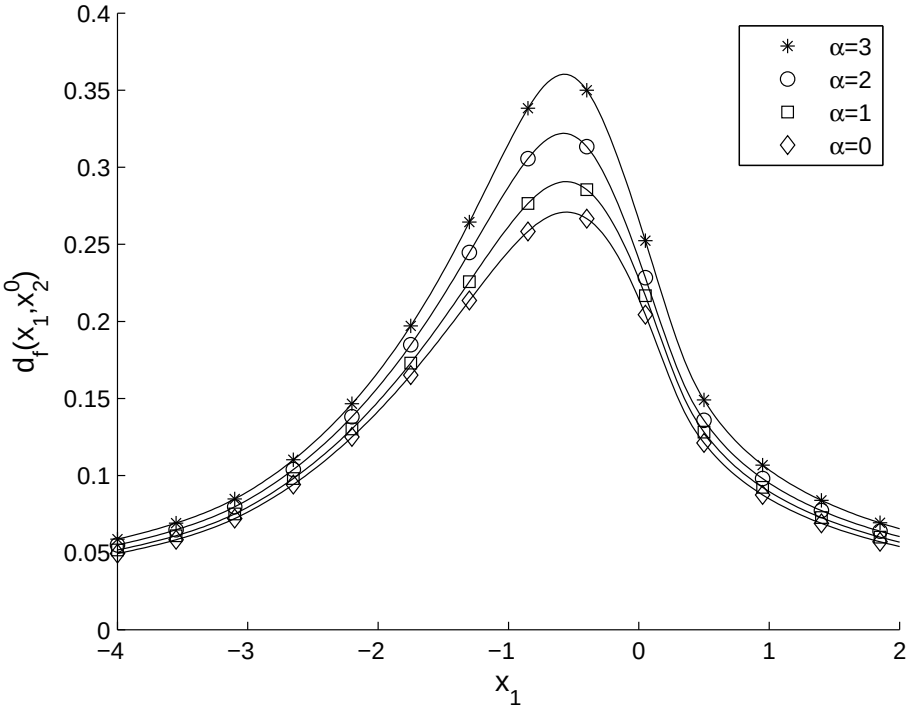

Fig. 24. Influence of the piezoviscosity over the (average) deformation

$\Delta d/d$	$\alpha = 1$	$\alpha = 2$	$\alpha = 3$
smooth	0.0540	0.1716	0.2787
$\varepsilon = 1/10$	0.0584	0.5742	0.6034
$\varepsilon = 1/20$	0.1078	0.2497	0.4532
$\varepsilon = 1/30$	0.0907	0.2198	0.4386
average	0.0732	0.1895	0.3320

Table 3
Maximum deformation elevation due to piezoviscosity

5 Conclusion

Numerical simulations of EHL problems are important for the design of both components and lubricants. On the one hand, th key numerical methods used in EHL solvers are the multigrid method [15] and multilevel multi-integration [16], which have proved robust and highly desirable in terms of reducing the time spent in solving EHL problems, at least for a moderated number of roughness patterns. On the other hand, accurate solutions of micro-EHL problems with realistic surface roughness requires such a high spatial resolution that even a single solution may be a large computational task [17]. Thus, as ε tends to 0, it seems more relevant to use the solution procedure that we have proposed because it deals with smooth coefficients. However, this average method may be coupled to multigrid methods (especially for the computation of the coefficients at the lowest grid resolution). The average method is valid for transverse or longitudinal roughness patterns. Further investigation has to be made in order to take into account anisotropic two dimensional effects.

References

[1] G. Bayada, J.-B. Faure, A double-scale analysis approach of the Reynolds roughness. Comments and application to the journal bearing, ASME J. Tribol. 111 (1989) 323–330.

[2] G. Bayada, S. Martin, C. Vázquez, Effets d'anisotropie par homogénéisation dans un problème à frontière libre, C. R. Math. Acad. Sci. Paris 340 (7) (2005) 541–546.

[3] G. Bayada, S. Martin, C. Vázquez, An average flow model of the Reynolds roughness including a mass-flow preserving cavitation model, ASME J. Tribol. 127 (4) (2005) 793–802.

[4] A. Kumar, J. F. Booker, A finite element cavitation algorithm, ASME J. Tribol. 113 (2) (1991) 276–86.

[5] F. Shi, R. F. Salant, A mixed soft elastohydrodynamic lubrication model with interasperity cavitation and surface shear deformation, ASME J. Tribol. 122 (2000) 308–316.

[6] D. Vijayaraghavan, T. G. Keith, An efficient, robust, and time accurate numerical scheme applied to a cavitation algorithm, ASME J. Tribol. 112 (1990) 44–51.

[7] H. G. Elrod, A cavitation algorithm, ASME J. Lubrication Technol. 103 (1981) 350–354.

[8] D. Dowson, G. R. Higginson, Elastohydrodynamic lubrication, Pergamon Press, Oxford, Great Britain, 1977.

[9] K. L. Johnson, Contact mechanics, Cambridge University Press, 1985.

[10] G. Bayada, S. Martin, C. Vázquez, Homogenization of a nonlocal elastohydrodynamic lubrication problem: a new free boundary model, Math. Mod. Meth. Appl. Sci. 15 (12) (2005) 1923–1956.

[11] G. Bayada, M. Chambat, C. Vázquez, Characteristics method for the formulation and computation of a free boundary cavitation problem, J. Comput. Appl. Math. 98 (2) (1998) 191–212.

[12] A. Bermúdez, J. Durany, La méthode des caractéristiques pour les problèmes de convection-diffusion stationnaires, RAIRO Modél. Math. Anal. Numér. 21 (1) (1987) 7–26.

[13] I. Arregui, J. J. Cendán, C. Vázquez, Mathematical analysis and numerical simulation of a Reynolds-Koiter model for the elastohydrodynamic journal-bearing device, M2AN Math. Model. Numer. Anal. 36 (2) (2002) 325–343.

[14] J. Durany, G. García, C. Vázquez, Numerical simulation of a lubricated Hertzian contact problem under imposed load, Finite Elem. Anal. Des. 38 (7) (2002) 645–658.

[15] C. H. Venner, A. A. Lubrecht, Multi-level methods in lubrication, Tribology and Interface Engineering Series, 37, Elsevier, 2000.

[16] A. Brandt, A. A. Lubrecht, Multilevel matrix multiplication and fast solution of integral equations, J. Comput. Phys. 90 (2) (1990) 348–370.

[17] A. A. Lubrecht, C. H. Venner, Elastohydrodynamic lubrication of rough surfaces, in: Proceedings of the Institution of Mechanical Engineers, Part J, Vol. 213, 1999, pp. 397–403.